

Comprehension of Multilingual Expressions Referring to Target Objects in Visual Inputs

Francisco Reis Nogueira
Instituto Superior Técnico

francisco.r.nogueira@tecnico.ulisboa.pt

Alexandre Bernardino
Instituto Superior Técnico

alexandre.bernardino@tecnico.ulisboa.pt

Bruno Emanuel da Graça Martins
Instituto Superior Técnico

bruno.g.martins@tecnico.ulisboa.pt

Abstract

Referring Expression Comprehension (REC) requires models to localize objects in images based on natural language descriptions. Research on the area remains predominantly English-centric, despite increasing global deployment demands. This work addresses multilingual REC through two main contributions. First, we construct a unified multilingual dataset spanning 10 languages, by systematically expanding 12 existing English REC benchmarks through machine translation and context-based translation enhancement. The resulting dataset comprises approximately 8 million multilingual referring expressions across 177,620 images, with 336,882 annotated objects. Second, we introduce an attention-anchored neural architecture that uses multilingual SigLIP2 encoders. Our attention-based approach generates coarse spatial anchors from attention distributions, which are subsequently refined through learned residuals. Experimental evaluation demonstrates competitive performance on standard benchmarks, e.g. achieving 86.9% accuracy at IoU@50 on RefCOCO aggregate multilingual evaluation, compared to an English-only result of 91.3%. Multilingual evaluation shows consistent capabilities across languages, establishing the practical feasibility of multilingual visual grounding systems. The dataset and model are available at multilingual.franreno.com

Keywords: *Referring Expression Comprehension, Multilingual Vision-Language Models*

1. Introduction

Humans can naturally identify objects in visual scenes from context dependent referring expressions. A simple phrase like “the red sports car” or a complex description like “the parked ketchup rocket” can both reference an object within

a visual scene. This capability extends across cultural and linguistic boundaries, with users adjusting expressions to accommodate common sense. In the context of visual and language research, this capability is studied through Referring Expression Comprehension (REC) tasks.

Addressing REC requires robust cross-modal understanding and spatial language grounding [28], through AI systems that must simultaneously parse linguistic information and accurately map it to visual cues within images. In this context, the development of encoder models based on Contrastive Language-Image Pre-training (CLIP) substantially improved text-image alignment, enabling progress in different vision and language tasks [22]. Multilingual CLIP (mCLIP) further extended these capabilities, enabling richer connections between multilingual text encoding and visual representations [6]. Current state-of-the-art vision and language encoder models, such as SigLIP2 [27], are also natively multilingual.

Despite the aforementioned advances, existing REC research faces a critical limitation. Nearly all benchmark datasets and trained models operate exclusively in English, which creates several fundamental limitations. First, referring expressions are inherently tied to linguistic structure, while spatial prepositions, adjective ordering, and descriptive conventions can vary significantly across languages. This means that models trained on English data may fail to generalize to other linguistic patterns. Second, simple machine translation introduces semantic shifts that can compromise grounding accuracy. Phrases that convey clear meaning in one language may become ambiguous when translated to English, or carry culturally distinct connotations that alter visual interpretation. Standard REC benchmarks such as RefCOCO [13] or RefCLEF [12], while providing essential evaluation frameworks, remain overwhelmingly monolingual. This limitation restricts research on cross-lingual grounding capabilities and prevents the devel-

opment of vision-language systems that can serve the global population in their native languages.

This work addresses these limitations through two main contributions: (1) a new multilingual dataset built by expanding 12 established English REC datasets into a unified multilingual corpus spanning 10 languages, and (2) an attention-anchored neural architecture to guide bounding box generation. The proposed model demonstrates competitive performance on standard benchmarks, while ensuring consistent multilingual capabilities. For instance, on RefCOCO [13], we achieve an averaged result of 91.3% IoU@50 in English evaluation, with a performance degradation of less than 8% all other languages. The model is particularly consistent among Romance languages (i.e., Spanish, French, Italian, and Portuguese), with mean IoU differences of only 2-4% compared to English. These results validate the feasibility of multilingual REC systems that can serve users in their native languages, without requiring language-specific architectural modifications.

The remainder of this paper is organized as follows: Section 2 reviews related work. Section 3 details our contributions, including the dataset construction through machine translation and content-aware quality enhancement (Section 3.1), and the attention-anchored neural network architecture (Section 3.2). Section 4 presents the experimental evaluation. Finally, Section 5 summarizes our findings and outlines directions for future work.

2. Related Work

Referring Expression Comprehension (REC) requires joint reasoning over the visual and linguistic modalities. This section reviews foundational developments in vision-language alignment, object detection architectures, and previous REC methods that inform our approach.

2.1. Vision-Language Foundation Models

Contrastive Language-Image Pre-training (CLIP) demonstrated that contrastive learning on large-scale image-text pairs produces powerful joint representations in a shared embedding space, enabling zero-shot transfer [22]. Multilingual extensions followed. For instance, mCLIP achieved cross-lingual vision-language alignment through triangular knowledge distillation from English-trained encoders to multilingual text encoders [6]. SigLIP refined the training approach by replacing the contrastive loss with a sigmoid loss, treating image-text matching as independent binary classification [38]. Building on this foundation, SigLIP2 incorporated decoder-based pretraining for localization tasks, different self-supervised losses, and multilingual data curation on the WebLI dataset spanning 100+ languages [27]. The SigLIP2 multilingual vision-language encoder provides the foundation for our attention-anchored architecture.

2.2. Object Detection and REC Architectures.

Previous REC methods build upon general object detection frameworks, adapting localization mechanisms for language-guided tasks. While traditional approaches like Faster R-CNN employed region proposal networks with predefined anchors [24], Detection Transformers (DETR) introduced learned object queries for end-to-end detection [5]. Subsequent work showed that anchor-based approaches remain effective when integrated with Transformers. For instance, DAB-DETR used dynamic anchor boxes as explicit positional queries that refine iteratively [15], while AnchorDETR demonstrated that learning to generate anchor points from queries enhances detection, particularly for small objects [33]. These findings established that anchors derived from learned representations, rather than fixed heuristics, can provide valuable inductive biases.

Early REC methods employed combinations of convolutional and recurrent networks but struggled with complex linguistic structures [20]. TransVG marked the transition to end-to-end Transformer architectures, reformulating visual grounding as direct coordinate regression and demonstrating that simple transformer stacks with self-attention over concatenated features outperform elaborate fusion mechanisms [8]. ReferFormer introduced the “*language as queries*” paradigm where linguistic expressions directly condition object queries, forcing focus on the referred object [34]. Recent architectures prioritize efficiency and open-vocabulary capabilities, for instance with Grounding DINO extending detection to open-set scenarios [16].

Despite these advances, multilingual visual grounding research remains limited. Referring expressions exhibit language-specific patterns in prepositions, adjective ordering, and descriptive conventions [30], while standard benchmarks like RefCOCO or RefCLEF remain overwhelmingly English-centric [12, 13]. Our architecture builds on attention-based spatial reasoning from transformer detection, while adapting these methods for multilingual deployment through frozen multilingual encoders.

3. The Proposed Approach to Multilingual Referring Expression Comprehension

This section presents our approach to multilingual REC. We first describe the construction of a unified multilingual dataset that systematically expands existing English REC benchmarks across 10 languages through translation, validation, and quality enhancement. We then introduce an attention-anchored neural architecture that uses multilingual vision-language encoders, together with efficient cross-modal enhancement and spatial attention mechanisms, for robust cross-lingual localization.

Table 1. Overview on the composition of the unified multilingual dataset, showing statistics for the 12 integrated benchmarks that, together, yield approximately 8M expressions across 177,620 images and 10 languages.

Dataset	Total Instances	Train	Validate	Test	Images	Objects	Expressions	EN Expressions	Image Source
RefOI	4,920	3,940	490	490	488	492	4,920	492	OpenImages
Multimodal Ground	8,550	7,040	740	770	2,550	855	8,550	855	Multimodal Ground
LocateBench	13,170	10,530	1,320	1,320	1,317	1,317	13,170	1,317	MS COCO
FG-OVD	23,490	9,390	13,560	6,780	1,707	2,349	23,490	2,349	MS COCO
RefDrone	170,330	123,360	14,210	32,760	7,971	16,938	170,330	17,033	VisDrone
Hindi Visual Genome	315,200	289,270	9,890	15,950	31,520	31,520	315,200	31,520	Visual Genome
Toloka	451,990	389,900	17,050	45,040	45,199	45,199	451,990	45,199	MS COCO
RefCOCOg	950,100	740,170	209,930	104,965	25,799	49,820	950,100	95,010	MS COCO
RefCLEF	1,303,640	1,140,980	25,030	37,630	19,997	29,985	1,303,640	130,364	SAIAPR-12
RefCOCO+	1,415,640	1,201,910	107,580	106,150	19,992	49,855	1,415,640	141,564	MS COCO
RefCOCO	1,422,100	1,384,470	10,340	27,290	19,944	49,999	1,422,100	142,210	MS COCO
FineCops-Ref	1,918,520	1,637,920	184,550	96,050	39,675	68,241	1,918,520	191,852	GQA
Overall	7,997,650	6,938,880	594,690	475,195	177,620	336,882	7,997,650	799,765	—

3.1. Dataset Collection and Integration

Our dataset construction methodology follows three guiding principles: (1) visual diversity, spanning everyday scenes, aerial imagery, fine-grained attributes, and compositional reasoning; (2) expression variety, ranging from concise phrases to elaborate descriptions and question-based formats; and (3) linguistic breadth, ensuring all English content correctly translates to 9 additional languages, while preserving referential accuracy.

We integrated 12 publicly available English datasets totaling 799,765 unique expressions across 177,620 images. This collection encompasses multiple visual domains and expression styles: the RefCOCO family provides standard everyday scene benchmarks with varying constraint sets [13]; RefCLEF adds natural stylistic variation through gameplay collection [12]; FineCops-Ref and FG-OVD test fine-grained attribute discrimination [3, 14]; RefDrone introduces aerial perspectives with small objects [26]; Hindi Visual Genome emphasizes ambiguous and underspecified references requiring contextual disambiguation [21]; RefOI isolates basic grounding without distractors, using single-presence instances [19]; Multimodal Ground targets instance-level product identification in controlled retail environments [18]; finally, Toloka VQA and LocateBench explore interrogative and multiple-choice formats [7, 29].

The integration provides 799,765 unique English expressions which we translated to 9 additional languages (Chinese, German, Dutch, Spanish, French, Italian, Korean, Portuguese, and Russian), yielding approximately 8 million total multilingual expressions across 177,620 images. All datasets were standardized to a unified JSON format, preserving bounding boxes in original pixel coordinates, image metadata, and dataset provenance. For datasets with existing train/validation/test splits, we mostly maintained the original partitions to ensure comparability with published baselines. However, in order to avoid contamination problems, we removed from the training split all the images that also occurred in the testing splits of other datasets. For LocateBench, which lacked predefined splits, we applied de-

terministic shuffling with a fixed random seed to create reproducible 80/10/10 train/validation/test divisions. In the case of FG-OVD and the Google variant of RefCOCOg, the official test partitions were unavailable in the original source distributions. To enable comprehensive evaluation while maintaining methodological rigor, we strategically allocated half of each validation set to serve as the corresponding test partition for these datasets. For RefCOCO and RefCOCO+, our test split aggregates the original testA and testB dataset splits.

After initial data collection we proceed through three stages: (1) translation of all English expressions to 9 languages using specialized multilingual models; (2) use of reference-free translation quality estimation to identify low-quality translations; (3) perform a multimodal enhancement that incorporates visual context for targeted improvement.

3.1.1. Machine Translation Methodology

We employed TowerInstruct-7B-v0.2, i.e. a multilingual language model which specializes on machine translation, as our primary translation engine [1]. TowerInstruct-7B handles multiple translation-related tasks including sentence-level translation, terminology-aware adaptation, and context-aware phrasing, making it well suited for referring expression translation.

We translated each English expression, in each source dataset, to all the considered 9 target languages (i.e., Chinese, German, Dutch, Spanish, French, Italian, Korean, Portuguese, and Russian), using a consistent prompt structure: "Translate to {target_language}.\n English: {text}\n {target_language}:". The complete translation process generated approximately 7.2 million translation pairs, producing a dataset of approximately 8M total multilingual referring expressions, including the English sources.

3.1.2. Quality Validation and Enhancement

We employed COMETkiwi-DA for reference-free translation quality evaluation, accessing and scoring the 7.2M translation pairs without any manual annotation [23]. Each

language had a quality threshold defined as the 40th percentile (P_{40}), with score distributions strongly right-skewed toward the 0.75-0.85 range. Translations scoring below the language-specific P_{40} threshold were flagged for targeted enhancement. Despite generally high quality scores, errors included over-literal translations losing the use of idiomatic expressions, translation failures generating contextually inappropriate responses, and semantic information loss omitting critical visual descriptors. These errors motivated the targeted enhancement strategy.

We re-translated the $\approx 3.7M$ expressions scoring below P_{40} (i.e., the lowest-quality 40% instances per language) using Google’s Gemini 2.0 Flash Lite with visual context included [10]. The enhancement pipeline processed each translation candidate using (1) the original English expression, (2) the initial text-only translation, and (3) the source image with the target object bounding box overlaid. A multimodal prompt instructed the Gemini model to improve translation quality by rephrasing while preserving meaning (see Appendix C1 for the complete prompt template).

Re-evaluation with COMETkiwi-DA demonstrated measurable improvements upon the enhancement across all languages, as shown on Figure that is given in Appendix C2, in the supplementary materials. Threshold gains ranged from +0.01 (in Portuguese, Russian, and Spanish) to +0.02 (in Chinese), with enhanced subset medians reaching 0.80-0.83. The enhanced mean scores clustered at 0.81-0.84, significantly above the original thresholds.

3.1.3. Characterization of the Resulting Dataset

The final unified dataset, summarized in Table 1, comprises approximately 8 million multilingual referring expressions across 10 languages, derived from approximately 800K unique English expressions over 177,620 distinct images with 336,882 annotated objects. The dataset features substantial diversity in visual domains (everyday scenes: 65%, aerial imagery: 2.1%, fine-grained attributes: 0.3%, instance-level objects: 4.1%) and expression complexity levels (simple single-object references: 15-20%, moderate 2-3 attributes/relations: 50-55%, complex compositional expressions: 25-30%). These statistics are derived from the original dataset characterizations, as given in the respective publications and content distributions.

3.2. A Neural Architecture for REC

We propose a new attention-anchored neural architecture for Referring Expression Comprehension (REC), which decomposes the localization task into coarse spatial attention, and learned fine-grained refinement. The model combines frozen SigLIP2 encoders with trainable cross-modal fusion modules and spatial attention layers, producing normalized bounding box coordinates directly from text-image pairs.

The architecture can be visualized in Figure 1, which illustrates the overall path that an input would take within the

model. Given an input image and a natural language referring expression, the model predicts a bounding box in normalized coordinates that localizes the referred object. Unlike in the context of multi-object detection tasks, our REC formulation requires identifying exactly one target object specified by the linguistic description, often requiring fine-grained discrimination among visually similar candidates. The proposed architecture processes inputs through five stages, which will be defined in the next sections.

3.2.1. Feature Extraction with SigLIP2

We use frozen SigLIP2 encoders¹ to extract aligned text and image representations. The text encoder processes tokenized sequences through transformer layers, producing contextualized representations for each token. The vision encoder divides 384x384 pixel images into 16×16 pixel patches, yielding a 24×24 grid of 576 visual tokens.

While most parts of the base SigLIP2 encoders remain frozen to preserve pre-trained visual-linguistic alignment, we unfreeze the final three layers of both the text and vision encoders. This selective fine-tuning allows task-specific adaptation of the encoders, while maintaining general semantic understanding, which corresponds to a critical balance for multilingual generalization [37].

Note that we have only used the base variant of the SigLIP2 model, envisioning deployment in resource constrained settings. Experiments with larger encoder models are left for future work.

3.2.2. Bidirectional Cross-Modal Fusion

A four-layer bidirectional Transformer iteratively refines initial alignments between text and image representations through parallel processing streams. Each layer contains four distinct attention mechanisms: (1) text self-attention, where text tokens attend to other text tokens; (2) text-to-image cross-attention, where text tokens query image patches; (3) image self-attention, where image patches attend to other patches; (4) and image-to-text cross-attention, where image patches query text tokens. Each attention operation is followed by feed-forward networks with residual connections and layer normalization.

3.2.3. Text Query Aggregation

After refinement with the cross-attention layers, we consolidate the distributed text representation into a single compact query vector. This aggregation employs masked mean pooling over valid text tokens to create a global text representation, followed by one feed-forward projection layer to transform the text representation into a query space. A learnable bias vector, associated to the feed-forward layer, provides task-specific initialization, this way breaking symmetry in the query representation.

¹<https://huggingface.co/google/siglip2-base-patch16-384>

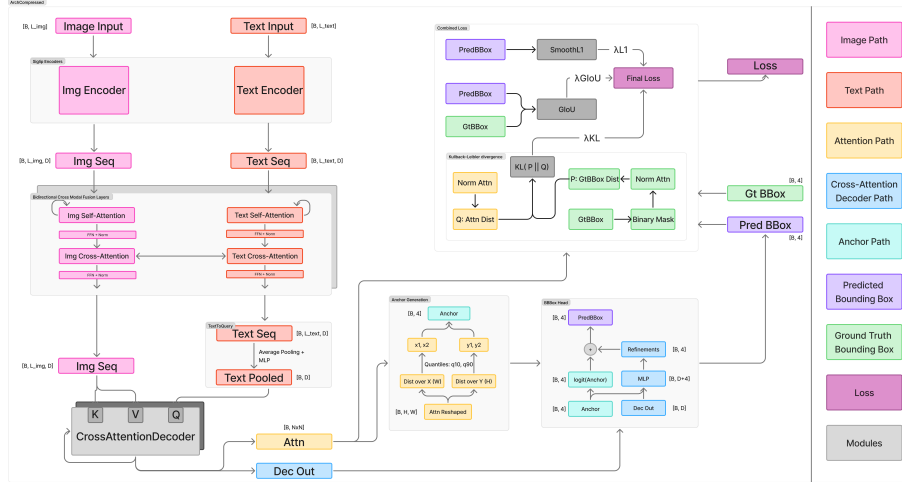


Figure 1. The proposed attention-anchored architecture, featuring a relatively small frozen SigLIP2 encoders, bidirectional cross-modal fusion, text query aggregation, a cross-attention decoder, and attention-guided bounding box prediction with residual refinement.

Notice that unlike object detection methods like DETR that use multiple learned queries for detecting various objects, our approach derives a single query directly from the natural language referring expression.

3.2.4. Cross-Attention Decoder Layers

Two stacked Transformer decoder layers refine the text query through repeated cross-attention with the image features, progressively enriching the query representation with spatially-grounded visual information. Each layer performs cross-attention from the query to image patches, followed by a feed-forward layer and also with residual connections and layer normalization operations.

Notice that the proposed architecture focuses computational resources on cross-modal attention, which directly contributes to spatial localization. Critically, each cross-attention operation produces attention weights representing a probability distribution over the 24×24 grid. These attention patterns can be used as foundation for our bounding box prediction approach, as described in the next section.

3.2.5. Attention-Anchored Grounding

Our bounding box regression decomposes prediction into coarse anchor generation from spatial attention patterns, followed by learned fine-grained refinement. The considered anchor generation operation is non-differentiable, and thus we supervise attention patterns via a KL divergence, teaching the model to produce distributions that naturally yield accurate bounding box anchors.

Cross-attention over the 24×24 grid produces normalized attention weights representing spatial confidence for each patch location. We consider the attention weights as a 2D distribution $A_{2D} \in \mathbb{R}^{24 \times 24}$ and marginalize to 1D distributions along horizontal and vertical axes:

$$p_x(x) = \sum_{y=1}^{24} A_{2D}(x, y), \quad p_y(y) = \sum_{x=1}^{24} A_{2D}(x, y). \quad (1)$$

After sharpening and re-normalizing the marginalized distributions through temperature scaling, we identify the spatial bounds of the predicted object by taking the 10th and 90th percentiles of the attention along each axis, capturing the central 80% of the attention mass. The anchor box is then defined as $(x_1, y_1, x_2 - x_1, y_2 - y_1)$, where x_1 and x_2 correspond to the normalized coordinates for the 10th and 90th percentiles of the cumulative horizontal distribution p_x , and y_1 and y_2 similarly correspond to the 10th and 90th percentiles of the cumulative vertical distribution p_y . This percentile-based definition yields a tight, adaptive anchor that reflects the spatial spread of attention while remaining robust to outliers and diffuse activations.

Notice that other procedures could also have been considered for generating the anchors (e.g., a bilinear interpolation of the attention weights into pixel coordinates, followed by greedy search to find the smallest bounding box that contains 80% of the attention). The procedure based on percentiles is nonetheless simpler, and it can be extended to use differentiable relaxations of sorting when computing the percentiles [4, 11], which is an option that we plan to consider as future work. Still, the current anchor generation process is non-differentiable, and thus we guide it through attention supervision separately from fine-grained refinement, which in turn is learned via coordinate losses.

Specifically, we use a two-layer MLP with rectifier activations to refine the anchors, by predicting bounded residuals $\delta \in [-1, 1]^4$. We apply residuals in logit space rather than coordinate space to ensure equal gradient magnitude

regardless of anchor position:

$$b_{pred} = \sigma(\text{logit}(b_{anchor}) + \delta). \quad (2)$$

In the previous expression, σ denotes the logistic sigmoid function, and $\text{logit}(x) = \log(x/(1-x))$. This logit-space formulation unwraps $[0, 1]$ coordinates to $(-\infty, \infty)$, providing stable gradients while constraining the final predictions to valid normalized coordinates. Unlike direct regression approaches that must learn full coordinate prediction from scratch, our method requires only learning residual adjustments over the attention-guided initial estimates.

3.2.6. Multi-Objective Loss Function

We train the model with three complementary loss components, weighted to balance coordinate accuracy, geometric overlap, and attention supervision:

$$\mathcal{L}_{total} = \lambda_{L1}\mathcal{L}_{L1} + \lambda_{GIoU}\mathcal{L}_{GIoU} + \lambda_{attn}\mathcal{L}_{attn}. \quad (3)$$

The three different components have weights of $\lambda_{L1} = 5.0$, $\lambda_{GIoU} = 2.0$, and $\lambda_{attn} = 0.2$.

The first component is a smooth L1 loss, which provides stable coordinate regression without the outlier sensitivity of the L2 loss, serving as the primary learning signal:

$$\mathcal{L}_{L1} = \frac{1}{N} \sum_{i=1}^N \text{smooth}_{L1}(\mathbf{b}_i^{pred} - \mathbf{b}_i^{gt}), \quad (4)$$

where

$$\text{smooth}_{L1}(x) = \begin{cases} 0.5x^2 & \text{if } |x| < 1 \\ |x| - 0.5 & \text{otherwise.} \end{cases} \quad (5)$$

The second component uses a generalized IoU (GIoU) score that directly optimizes geometric overlap between predicted and ground truth bounding boxes, by extending the standard IoU to provide meaningful gradients even for non-overlapping cases [25]. It is defined as follows:

$$\text{GIoU} = \text{IoU} - \frac{|C \setminus (A \cup B)|}{|C|}, \quad (6)$$

where A and B denote the predicted and ground truth bounding boxes, and where C is the smallest enclosing box covering both A and B . The second term penalizes the normalized area outside the union of A and B , encouraging the predicted bounding box to move closer to the ground truth even when the IoU is equal to 0. The corresponding loss is $\mathcal{L}_{GIoU} = 1 - \text{GIoU}$, providing a more stable optimization signal than the standard IoU.

Finally, the attention supervision loss explicitly teaches the model where to look given a referring expression, supporting our attention-anchored prediction approach. We

convert the ground-truth bounding box into a binary target map over the 24×24 grid by assigning $r_i = 1$ for patches inside the box and $r_i = 0$ otherwise. This binary mask is normalized to form the optimization target with a probability distribution p_{target} over the 576 patches. The loss minimizes the KL divergence between predicted attention a_{norm} and this target distribution:

$$\mathcal{L}_{attn} = \sum_{i=1}^{576} p_{target}(i) \log \frac{p_{target}(i)}{a_{norm}(i)}. \quad (7)$$

The previous expression guides the model on where to look given a referring expression. Accurate attention patterns produce better anchor boxes, which in turn simplify the bounding box refinement task.

4. Experimental Evaluation

We evaluate the attention-anchored model across three different dimensions: aggregate performance on the complete multilingual test set, dataset-specific analysis to assess coverage of different domains, and per-language assessment quantifying multilingual consistency.

Training was performed on a single NVIDIA RTX 4090 with batch size 32 and mixed-precision. We used AdamW with weight decay of 0.01 and gradient clipping with norm 1.0 [17]. Learning rates are 10^{-6} for the SigLIP2 encoder’s top layers, 10^{-5} for cross-modal fusion, and 10^{-4} for the task-specific components. Evaluation covers 429,154 referring expressions across all test splits. Metrics include mean IoU (mIoU) and IoU@50. Results are analyzed globally, per dataset, and per language, to examine localization quality and multilingual generalization.

4.1. Aggregate Performance

We evaluated the attention-anchored model on the 429,154 test expressions from the complete dataset. Several of the sub-datasets nonetheless require evaluation clarifications. For instance, FG-OVD and RefCOCOg lack official test splits, so we reserved half of their validation sets for testing. Hindi Visual Genome and RefOI were excluded from the detailed presentation in Table 2 due to absence of published REC baselines and methodological inconsistencies with multi-object evaluation protocols, respectively. For RefCOCO and RefCOCO+, we did not distinguish between the original testA and testB splits, and instead merged them into a single test set for evaluation. To enable a fair comparison with previous studies that report separate results for each split, we adjusted the reported accuracies using a weighted average based on the number of samples in each test subset. Finally, RefCOCOg split was compared only for its reported validation score.

Table 2 presents the overall results, together with a comparative performance assessment for some of the sub-

Table 2. Comparison of the attention-anchored model with state-of-the-art referring expression comprehension methods across multiple English benchmark datasets. The second column lists previously published models evaluated on each dataset, which we use as baselines for comparison. Results are reported in two configurations: aggregate multilingual (A), combining all 10 languages, and English-only (E) evaluation. Best results for each metric are shown in bold, while dashes (–) indicate metrics not reported in the original publications.

Dataset	Baseline English Method	IoU@50		mIoU	
		Baseline	Ours (A / E)	Baseline	Ours (A / E)
FG-OVD	Detic [3, 39]	0.697	0.512 / 0.565	–	0.463 / 0.509
FineCops-Ref	CogVLM [14]	0.782	0.568 / 0.603	–	0.520 / 0.550
LocateBench	GPT-4o [7]	0.604	0.552 / 0.614	–	0.528 / 0.577
Multimodal Ground	MRVG-NET [18]	0.807	0.544 / 0.532	0.798	0.458 / 0.489
RefCLEF	LMSVA [36]	0.730	0.618 / 0.681	–	0.565 / 0.612
RefCOCO	CogVLM [32]	0.920	0.869 / 0.913	–	0.788 / 0.822
	Grounding DINO [16]	0.908			
	OFA-Large [31]	0.893			
	Qwen-VL [2]	0.886			
	UNINEXT-H [35]	0.824			
RefCOCO+	CogVLM	0.885	0.689 / 0.746	–	0.637 / 0.634
	Grounding DINO	0.827			
	OFA-Large	0.849			
	Qwen-VL	0.831			
	UNINEXT-H	0.712			
RefCOCOg	CogVLM	0.897	0.765 / 0.793	–	0.699 / 0.720
RefDrone	NGDINO-T [26]	0.218	0.236 / 0.257	–	0.225 / 0.241
Toloka	wtxy89 [9]	0.834	0.583 / 0.626	0.763	0.502 / 0.535
Overall	–	–	0.625 / 0.672	–	0.571 / 0.609

datasets against previously published state-of-the-art baselines, reporting results in two configurations, namely aggregate multilingual (A) and English-only (E). The proposed model achieves a mean IoU of 0.571 and a median of 0.721 across the complete test set. Accuracy metrics show that 62.5% of the predictions exceed the IoU threshold of 0.5, while 50.1% exceed the stricter threshold of 0.7. The gap between the mean (0.571) and the median (0.721) indicates a right-skewed score distribution.

4.2. Dataset-Level Performance

Performance varies substantially across the original English datasets. The instances from the RefCOCO family have the strongest results: RefCOCO has 0.788 mean IoU (86.9% IoU@50, 80.8% IoU@70), while RefCOCO+ has 0.637 mean IoU (68.9% IoU@50, 61.9% IoU@70). RefCLEF has 0.565 mean IoU (61.8% IoU@50), and FineCops-Ref has 0.520 mean IoU (56.8% IoU@50). RefDrone exhibits markedly lower performance with 0.225 mean IoU (23.6% IoU@50, median 0.022). Toloka VQA has 0.502 mean IoU (58.3% IoU@50), and Hindi Visual Genome has 0.435 mean IoU (46.7% IoU@50). LocateBench has 0.528 mean

IoU (55.2% IoU@50), while Multimodal Ground has 0.458 mean IoU (54.4% IoU@50).

Compared to published baselines, our model achieves competitive performance. For instance, on RefCOCO, we surpass the Grounding Dino [16] baseline and perform similarly to the much larger CogVLM model [32]. For RefDrone, we improve over the NGDINO-T baseline [26], demonstrating progress on the challenging aerial domain despite the absolute performance remaining low. However, significant gaps persist on Toloka VQA (83.4% for the best system in the competition vs. 62.6% for ours) and Multimodal Ground (80.7% vs. 53.2%). On LocateBench, we slightly exceed the GPT-4o baseline (60.4% vs. 61.4%), validating effectiveness on multiple-choice localization, despite the different task format. It is important to note that our evaluation on RefOI employed the single-occurrence mode exclusively. Consequently, direct quantitative comparison with published results is not feasible, as the original benchmarks incorporate both single-occurrence and multi-occurrence evaluation protocols. An additional discussion on the per-dataset results is given in Appendix B1.

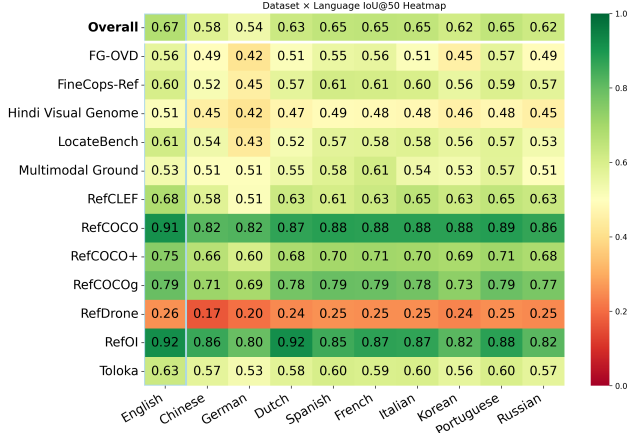


Figure 2. Multilingual performance in terms of IoU@50 across datasets and languages. Rows represent datasets, while columns represent languages. Green indicates higher IoU@50.

4.3. Multilingual Performance

Figure 2 presents per-language performance across all datasets using IoU@50 as the evaluation metric.

English establishes the performance ceiling at 63.8% IoU@50, with other languages exhibiting relatively modest degradation. Romance languages cluster within a narrow band, with Spanish (61.3% IoU@50), French (61.4% IoU@50), Italian (61.3% IoU@50), and Portuguese (61.3% IoU@50) achieving near-identical performance, differing by at most 0.1 percentage points from the English results.

Germanic languages show greater variation, with Dutch achieving 59.2% IoU@50, and German reaching 50.8% IoU@50. Russian obtains 59.1% IoU@50, while East Asian languages demonstrate 58.7% IoU@50 for Korean, and 55.5% IoU@50 for Chinese.

Performance gaps between English and other languages thus range from 2.5 percentage points (Italian: 63.8% vs. 61.3%) to 13 percentage points (German: 63.8% vs. 50.8%) in terms of the IoU@50 metric. An additional discussion on the multilingual performance is given in Appendix B2.

4.4. Attention-Anchored vs. Direct Regression

To validate the contribution of the attention-anchored prediction mechanism, we compared our complete approach against a baseline variant that uses direct regression, to isolate the impact of anchor generation and residual refinement. Both models share the same cross-attention decoder, differing only in the final prediction head.

Table 3 reports the IoU@50 score across 10 of the sub-datasets and also overall. The attention-anchored approach consistently outperforms direct regression, yielding mean gains of +11.3 percentage points in the multilingual evaluation, and +8 in the English-only evaluation. Improvements are more pronounced on datasets with small or visu-

Table 3. Results from an ablation study comparing the attention-anchored approach against direct regression, using the IoU@50 metric. Results are reported for aggregate multilingual (A) and English-only (E) evaluation. Best results for each configuration are shown in **bold**, while the Δ columns show the percentage point difference between the strategies.

Dataset	Attn-Anch.		Direct-Reg.		Δ	
	A	E	A	E	A	E
RefCOCO	86.9	91.3	79.4	87.7	+7.5	+3.6
RefCOCO+	68.9	74.6	57.8	62.9	+11.1	+11.7
RefCOCOg	76.5	79.3	65.2	69.3	+11.3	+10.0
RefCLEF	61.8	68.1	56.8	62.8	+5.0	+5.3
RefDrone	23.6	25.7	7.5	8.8	+16.1	+16.9
RefOI	85.8	91.8	86.3	88.0	-0.5	+3.8
Toloka	58.3	62.6	45.4	48.6	+12.9	+14.0
LocateBench	55.2	61.4	41.4	44.6	+13.8	+16.8
FineCops-Ref	56.8	60.3	48.3	51.8	+8.5	+8.5
Multimodal Ground	54.4	53.2	21.6	23.4	+32.8	+29.8
Hindi VG	46.7	50.8	41.8	46.8	+4.9	+4.0
FG-OVD	51.2	56.5	36.9	42.4	+14.3	+14.1
Overall	62.5	67.2	54.2	59.2	+11.3	+8

ally complex targets, such as Multimodal Ground (+32.8). RefOI is the single case where direct regression slightly surpasses anchored prediction in terms of the aggregate evaluation (-0.5), although the anchored approach remains superior in the English-only evaluation. Qualitative examples are given in Appendix D, in the supplementary materials.

5. Conclusions and Future Work

This work established foundational infrastructure for multilingual Referring Expression Comprehension (REC) through two primary contributions: (1) a unified multilingual dataset expanding 12 English REC benchmarks across 10 languages through systematic translation, quality validation, and visual context enhancement, yielding 8M multilingual referring expressions; and (2) an attention-anchored neural architecture that decomposes localization into coarse spatial attention and learned refinement, achieving language-agnostic grounding through frozen multilingual encoders and interpretable attention mechanisms.

Performance with the proposed model is competitive over multiple individual English-centric baselines, while achieving generalization to multiple languages and domains, validating the feasibility of multilingual REC methods that can serve users in their native languages, without language-specific architectural modifications.

Key limitations include (1) the non-differentiable anchor generation procedure requiring explicit attention supervision via KL divergence, potentially limiting extension to multi-object scenarios, (2) spatial resolution constraints from the 16×16 pixel patch granularity, preventing sub-patch localization precision for small objects, and (3) the single-object prediction constraint, where plural expressions referencing multiple instances result in selecting only

one target encompassing bounding box.

Future work can explore multi-scale feature extraction for improved small object handling, as well as alternative anchor generation methods as discussed in section 3.2.5. We also plan to extend the dataset to additional languages and specialized domains (e.g., medical or satellite imagery).

References

- [1] Duarte M. Alves, José Pombal, Nuno M. Guerreiro, Pedro H. Martins, João Alves, Amin Farajian, Ben Peters, Ricardo Rei, Patrick Fernandes, Sweta Agrawal, Pierre Colombo, José G. C. de Souza, and André F. T. Martins. Tower: An open multilingual large language model for translation-related tasks. In *EMNLP*, 2024. 3
- [2] Jinze Bai, Shuai Bai, Shusheng Yang, Shijie Wang, Sinan Tan, Peng Wang, Junyang Lin, Chang Zhou, and Jingren Zhou. Qwen-vl: A versatile vision-language model for understanding, localization, text reading, and beyond. *arXiv preprint arXiv:2308.12966*, 2023. 7
- [3] Lorenzo Bianchi, Fabio Carrara, Nicola Messina, Claudio Gennaro, and Fabrizio Falchi. The devil is in the fine-grained details: Evaluating open-vocabulary object detectors for fine-grained understanding. In *CVPR*, 2024. 3, 7
- [4] Mathieu Blondel, Olivier Teboul, Quentin Berthet, and Josip Djolonga. Fast differentiable sorting and ranking. In *ICML*, 2020. 5
- [5] Nicolas Carion, Francisco Massa, Gabriel Synnaeve, Nicolas Usunier, Alexander Kirillov, and Sergey Zagoruyko. End-to-end object detection with transformers. In *ECCV*, 2020. 2
- [6] Guanhua Chen, Lu Hou, Yun Chen, Wenliang Dai, Lifeng Shang, Xin Jiang, Qun Liu, Jia Pan, and Weping Wang. mCLIP: Multilingual CLIP via cross-lingual transfer. In *ACL*, 2023. 1, 2
- [7] Ting-Rui Chiang, Joshua Robinson, Xinyan Velocity Yu, and Dani Yogatama. Locatebench: Evaluating the locating ability of vision language models. *arXiv preprint arXiv:2410.19808*, 2024. 3, 7
- [8] Jiajun Deng, Zhengyuan Yang, Tianlang Chen, Wengang Zhou, and Houqiang Li. Transvg: End-to-end visual grounding with transformers. In *ICCV*, 2021. 2
- [9] Shengyi Gao, Zhe Chen, Guo Chen, Wenhai Wang, and Tong Lu. Champion solution for the 2023 toloka vqa challenge. *arXiv preprint arXiv:2301.09045*, 2023. 7
- [10] Google DeepMind. Gemini 2.0 flash experimental, 2025. Available at <https://ai.google.dev/gemini-api/docs/models>. 4
- [11] Aditya Grover, Eric Wang, Aaron Zweig, and Stefano Ermon. Stochastic optimization of sorting networks via continuous relaxations. In *ICLR*, 2019. 5
- [12] Sahar Kazemzadeh, Vicente Ordonez, Mark Matten, and Tamara Berg. ReferItGame: Referring to objects in photographs of natural scenes. In *EMNLP*, 2014. 1, 2, 3
- [13] Tsung-Yi Lin, Michael Maire, Serge Belongie, Lubomir Bourdev, Ross Girshick, James Hays, Pietro Perona, Deva Ramanan, C. Lawrence Zitnick, and Piotr Dollár. Microsoft COCO: Common objects in context. In *ECCV*, 2014. 1, 2, 3
- [14] Junzhuo Liu, Xuzheng Yang, Weiwei Li, and Peng Wang. FineCops-Ref: A new dataset and task for fine-grained compositional referring expression comprehension. In *EMNLP*, 2024. 3, 7
- [15] Shilong Liu, Feng Li, Hao Zhang, Xiao Yang, Xianbiao Qi, Hang Su, Jun Zhu, and Lei Zhang. DAB-DETR: Dynamic anchor boxes are better queries for DETR. In *ICLR*, 2022. 2
- [16] Shilong Liu, Zhaoyang Zeng, Tianhe Ren, Feng Li, Hao Zhang, Jie Yang, Qing Jiang, Chunyuan Li, Jianwei Yang, Hang Su, et al. Grounding dino: Marrying dino with grounded pre-training for open-set object detection. In *ECCV*, 2024. 2, 7
- [17] Ilya Loshchilov and Frank Hutter. Decoupled weight decay regularization. In *ICLR*, 2019. 6
- [18] Yangxiao Lu, Ruosen Li, Liqiang Jing, Jikai Wang, Xinya Du, Yunhui Guo, Nicholas Ruoizzi, and Yu Xiang. Multimodal reference visual grounding. *arXiv preprint arXiv:2504.02876*, 2025. 3, 7
- [19] Ziqiao Ma, Jing Ding, Xuejun Zhang, Dezhi Luo, Ji-ah Ding, Sihan Xu, Yuchen Huang, Run Peng, and Joyce Chai. Vision-language models are not pragmatically competent in referring expression generation. *arXiv preprint arXiv:2504.16060*, 2025. 3
- [20] Junhua Mao, Jonathan Huang, Alexander Toshev, Oana Camburu, Alan L Yuille, and Kevin Murphy. Generation and comprehension of unambiguous object descriptions. In *CVPR*, 2016. 2
- [21] Shantipriya Parida, Ondřej Bojar, and Satya Ranjan Dash. Hindi visual genome: A dataset for multimodal english-to-hindi machine translation. *arXiv preprint arXiv:1907.08948*, 2019. 3
- [22] Alec Radford, Jong Wook Kim, Chris Hallacy, Aditya Ramesh, Gabriel Goh, Sandhini Agarwal, Girish Sastry, Amanda Askell, Pamela Mishkin, Jack Clark, Gretchen Krueger, and Ilya Sutskever. Learning transferable visual models from natural language supervision. In *ICML*, 2021. 1, 2
- [23] Ricardo Rei, Marcos Treviso, Nuno M. Guerreiro, Chrysoula Zerva, Ana C Farinha, Christine Maroti, José G. C. de Souza, Taisiya Glushkova, Duarte Alves,

- Luisa Coheur, Alon Lavie, and André F. T. Martins. CometKiwI: IST-unbabel 2022 submission for the quality estimation shared task. In *WMT*, 2022. 3
- [24] Shaoqing Ren, Kaiming He, Ross Girshick, and Jian Sun. Faster R-CNN: Towards real-time object detection with region proposal networks. In *NeurIPS*, 2015. 2
- [25] Hamid Reza Tofighi, Nathan Tsoi, JunYoung Gwak, Amir Sadeghian, Ian Reid, and Silvio Savarese. Generalized intersection over union. *CVPR*, 2019. 6
- [26] Zhichao Sun, Yepeng Liu, Huachao Zhu, Yuliang Gu, Yuda Zou, Zelong Liu, Gui-Song Xia, Bo Du, and Yongchao Xu. RefDrone: A challenging benchmark for referring expression comprehension in drone scenes. *arXiv preprint arXiv:2502.00392*, 2025. 3, 7
- [27] Michael Tschanen, Alexey Gritsenko, Xiao Wang, Muhammad Ferjad Naeem, Ibrahim Alabdulmohsin, Nikhil Parthasarathy, Talfan Evans, Lucas Beyer, Ye Xia, Basil Mustafa, Olivier Hénaff, Jeremiah Harmsen, Andreas Steiner, and Xiaohua Zhai. SigLIP 2: Multilingual vision-language encoders with improved semantic understanding, localization, and dense features. *arXiv preprint arXiv:2502.14786*, 2025. 1, 2
- [28] Akshar Tumu, Varad Shinde, and Parisa Kordjamshidi. Referring expressions as a lens into spatial language grounding in vision-language models. In *IJCNLP-AAACL*, 2025. 1
- [29] Dmitry Ustalov, Nikita Pavlichenko, Sergey Koshelev, Daniil Likhobaba, and Alisa Smirnova. Toloka visual question answering benchmark. In *WSDM Cup*, 2023. 3
- [30] Brandon Waldon and Judith Degen. Modeling cross-linguistic production of referring expressions. In *SCiL*, 2021. 2
- [31] Peng Wang, An Yang, Rui Men, Junyang Lin, Shuai Bai, Zhikang Li, Jianxin Ma, Chang Zhou, Jingren Zhou, and Hongxia Yang. Ofa: Unifying architectures, tasks, and modalities through a simple sequence-to-sequence learning framework. In *ICML*, 2022. 7
- [32] Weihang Wang, Qingsong Lv, Wenmeng Yu, Wenyi Hong, Ji Qi, Yan Wang, Junhui Ji, Zhuoyi Yang, Lei Zhao, Song XiXuan, et al. CogVLM: Visual expert for pretrained language models. *NeurIPS*, 2024. 7
- [33] Yingming Wang, Xiangyu Zhang, Tong Yang, and Jian Sun. Anchor DETR: Query design for transformer-based object detection. In *AAAI*, 2022. 2
- [34] Jiannan Wu, Yi Jiang, Peize Sun, Zehuan Yuan, and Ping Luo. Language as queries for referring video object segmentation. In *CVPR*, 2022. 2
- [35] Bin Yan, Yi Jiang, Jiannan Wu, Dong Wang, Ping Luo, Zehuan Yuan, and Huchuan Lu. Universal instance perception as object discovery and retrieval. In *CVPR*, 2023. 7
- [36] Haibo Yao, Lipeng Wang, Chengtao Cai, Wei Wang, Zhi Zhang, and Xiaobing Shang. Language conditioned multi-scale visual attention networks for visual grounding. *Image and Vision Computing*, 150:105242, 2024. 7
- [37] Jason Yosinski, Jeff Clune, Yoshua Bengio, and Hod Lipson. How transferable are features in deep neural networks? In *NeurIPS*, 2014. 4
- [38] Xiaohua Zhai, Basil Mustafa, Alexander Kolesnikov, and Lucas Beyer. Sigmoid loss for language image pre-training. In *ICCV*, 2023. 2
- [39] Xingyi Zhou, Rohit Girdhar, Armand Joulin, Philipp Krähenbühl, and Ishan Misra. Detecting twenty-thousand classes using image-level supervision. In *ECCV*, 2022. 7

Appendix A: Important Limitations and Ethical Considerations

While our model aims to contribute to research beyond English-centric referring expression comprehension, it has limitations in that the results are only conditioned on, and evaluated on, machine translated data from existing English-centric datasets. This fundamental constraint means that despite our efforts to enhance translation quality through visual context-based refinement, the multilingual dataset inherits potential biases and limitations from both the original English-language sources and the translation process itself. Machine translation, even when enhanced with multimodal grounding, cannot fully capture the nuanced ways different linguistic communities naturally describe visual scenes, as referring expression conventions reflect cultural and linguistic patterns that may not transfer directly through translation.

The data used in our experiments is also limited in the coverage of geographically diverse concepts, reflecting the predominantly Western-centric nature of the underlying image collections (i.e., MS COCO, Visual Genome, or Open-Images). Objects, scenes, and spatial arrangements common in other global contexts may be underrepresented or absent entirely, potentially limiting the model’s effectiveness when deployed in diverse real-world settings. Even our visual context-based refinement procedure, while improving translation quality measurably, is not fully capable of avoiding problems inherent to automatic machine translation, such as loss of pragmatic meaning, cultural connotations, or language-specific spatial reasoning patterns documented in linguistic literature.

Future work in this area should invest further in the annotation and curation of truly multilingual data for referring expression comprehension, ideally collected from na-

tive speakers describing images relevant to their own cultural contexts. This would involve expanding the range of covered languages beyond our current ten-language scope, particularly to include low-resource languages and linguistic families not represented in our dataset (e.g., African, Indigenous, and Southeast Asian languages). Additionally, research should explore how referring expression conventions vary across culture, and whether vision-language models can learn these language-specific patterns rather than imposing English-centric spatial reasoning universally.

Appendix B: Additional Discussion

We further discuss here the per-dataset performance and the multilingual results.

Appendix B1: Per-Dataset Analysis

The experimental results demonstrate competitive performance on standard benchmarks. For instance, RefCOCO achieves an averaged result of 86.9% IoU@50, and RefCOCO+ obtains 68.9% IoU@50. The strong performance on the RefCOCO family validates that our attention-anchored approach effectively handles diverse referring expression styles and complex scenes with multiple objects. Moreover, the gap between mean (0.540) and median (0.689) IoU reflects a right-skewed distribution where most predictions achieve strong localization, while domain-specific challenges contribute to lowering the aggregate mean.

RefDrone’s aerial imagery presents the most significant challenge (0.225 mean IoU), likely due to three factors: (1) non-standard overhead viewpoints that differ from the predominantly ground-level perspectives in the SigLIP2 pre-training data; (2) small object scales (31.1% small targets) that occupy few patches in our 24×24 grid, making percentile-based anchor generation less reliable; (3) occlusions and viewing angle variations that create ambiguous spatial relationships. These results suggest future work should incorporate multi-scale feature extraction or adaptive grid resolutions for small object handling.

Appendix B2: Multilingual Analysis

The multilingual evaluation reveals two key findings. Romance languages (Spanish, French, Italian, and Portuguese) achieve remarkably consistent performance, with mean IoU clustering tightly around 0.556, validating our visual context-based translation enhancement. This consistency likely stems from shared linguistic structures (adjective-noun ordering, or preposition usage) and the high quality of the Romance language translations resulting from our automatic enhancement pipeline.

Performance gaps between English (0.577) and other languages remain modest, typically less than 8%, with two

notable exceptions, namely German (12.7% gap) and Chinese (9.6% gap). German’s larger gap may reflect structural differences in compound nouns and spatial prepositions that create translation challenges, while Chinese’s gap aligns with its lower translation quality baseline.

Appendix C: Details on the Translation Enhancement Methodology

This appendix provides complete implementation details for the visual context-based translation enhancement pipeline, which elevated baseline translation quality across all target languages. We present the full prompt template employed with Google’s Gemini 2.0 Flash Lite model and analyze the resulting quality improvements.

C.1: Visual Context-Based Prompt Template

The translation enhancement pipeline employed the following prompt template with Google’s Gemini 2.0 Flash Lite model. Each instance received three inputs: the original English expression, the initial text-only translation, and the source image with a target object bounding box overlay.

```
You are a translation-quality-improvement assistant.

Original Text in English: {expression_text}

Translation to {language_code}: {translation}

Instruction: Given the original text and its translation
, and taking the image as context, improve the
quality of the translation by rephrasing it. Ensure
the rephrased translation closely aligns with the
original text in meaning, structure, tone, and
style. Make the rephrased translation sound natural
and fluent in the target language while preserving
all essential details, correcting any grammatical
errors, and retaining all stylistic elements. The
rephrased translation should not be ambiguous,
avoiding terms that can have a double meaning in
the target language, or qualifying these terms with
sufficient details for disambiguation.
```

C.2: Quality Distribution Improvements

Figure 3 presents the distribution of COMETkiwi-DA scores before and after visual context-based enhancement across the nine target languages. The histograms reveal consistent rightward shifts across all languages, indicating systematic quality improvements through visual enhancement. Chinese demonstrates the most substantial distributional shift, with the enhanced distribution (teal) showing marked concentration in higher quality ranges compared to the baseline (coral). This improvement is particularly significant given Chinese’s initial lower performance ($P_{40} = 0.748$), where 40.9% of the baseline translations scored below 0.75. The P_{40} thresholds, marked by vertical dashed lines, visually capture the magnitude of improvement, with Chinese showing the largest gap between baseline and enhanced thresholds, followed by Portuguese and Russian.

Language family patterns observed in baseline quality

persist through enhancement, though with notable convergence. Romance languages (i.e., Spanish, French, Italian, and Portuguese) maintain their quality clustering while achieving consistent improvements, with all four languages shifting their distributions rightward. Germanic languages (i.e., German, and Dutch) and Korean, which exhibited stronger baseline performance, show more modest but meaningful shifts, suggesting that visual enhancement benefits lower-performing translations disproportionately. The reduced left-tail mass across all distributions indicates that enhancement particularly addresses the 26.5% of baseline translations scoring below 0.75, elevating problematic translations toward acceptable quality thresholds while maintaining the integrity of already high-quality translations.

Appendix D: Qualitative Analysis

This appendix provides visual evidence for successful or problematic referring expression comprehension localizations, demonstrating the model’s capabilities across diverse linguistic and visual scenarios. We present a collection of figures that illustrate both the strengths and limitations of the attention-anchored architecture through carefully selected examples, spanning multilingual consistency, compositional reasoning patterns, attribute-based discrimination, and challenging failure modes.

Multilingual consistency is demonstrated in Figures 4, 6, and 10, showing that spatial predictions remain stable across language families, despite structural differences in referring expressions. For instance, Figure 4 presents a wine tasting scene where the model accurately localizes the second wine glass from the left when queried in Russian, English, and Italian, spanning three distinct language families (Slavic, Germanic, and Romance), with nearly identical spatial predictions across all three languages. This cross-lingual stability extends to various object categories and scene complexities, validating the language-agnostic nature of the learned spatial representations.

Compositional reasoning capabilities are illustrated through ordinal counting (Figure 7), multi-hop spatial relationships (Figure 9), negation handling (Figure 11), and fine-grained discrimination, including relative size (Figure 13), color differentiation (Figure 17), and semantic disambiguation (Figure 18). In turn, Figure 5 demonstrates the model’s ability to disambiguate multiple objects within the same office scene through combined attribute descriptions: identifying an earphone by material and color properties, a cup by color and text pattern, and a glass container by material characteristics. These examples collectively validate that the architecture achieves language-agnostic spatial reasoning and complex compositional understanding beyond simple attribute matching.

Small object localization across diverse domains is pre-

sented in Figures 8 and 15, illustrating that difficulty correlates with both object size and contextual clutter.

Figure 12 reveals how attention distributions guide anchor generation, demonstrating interpretable spatial patterns aligned with human intuitions. In complement to this, a qualitative ablation study (Figure 16) shows that attention-anchored prediction consistently outperforms direct regression, particularly for small objects and cluttered scenes, validating the architectural decomposition into coarse attention-based anchors followed by learned refinement. Finally, Figure 14 illustrates failure cases where attention spreads across multiple objects, particularly with plural references, suggesting that explicit singular-plural modeling and improved distractor suppression represent important directions for future work.

Translation Quality Distributions: Original vs Enhanced

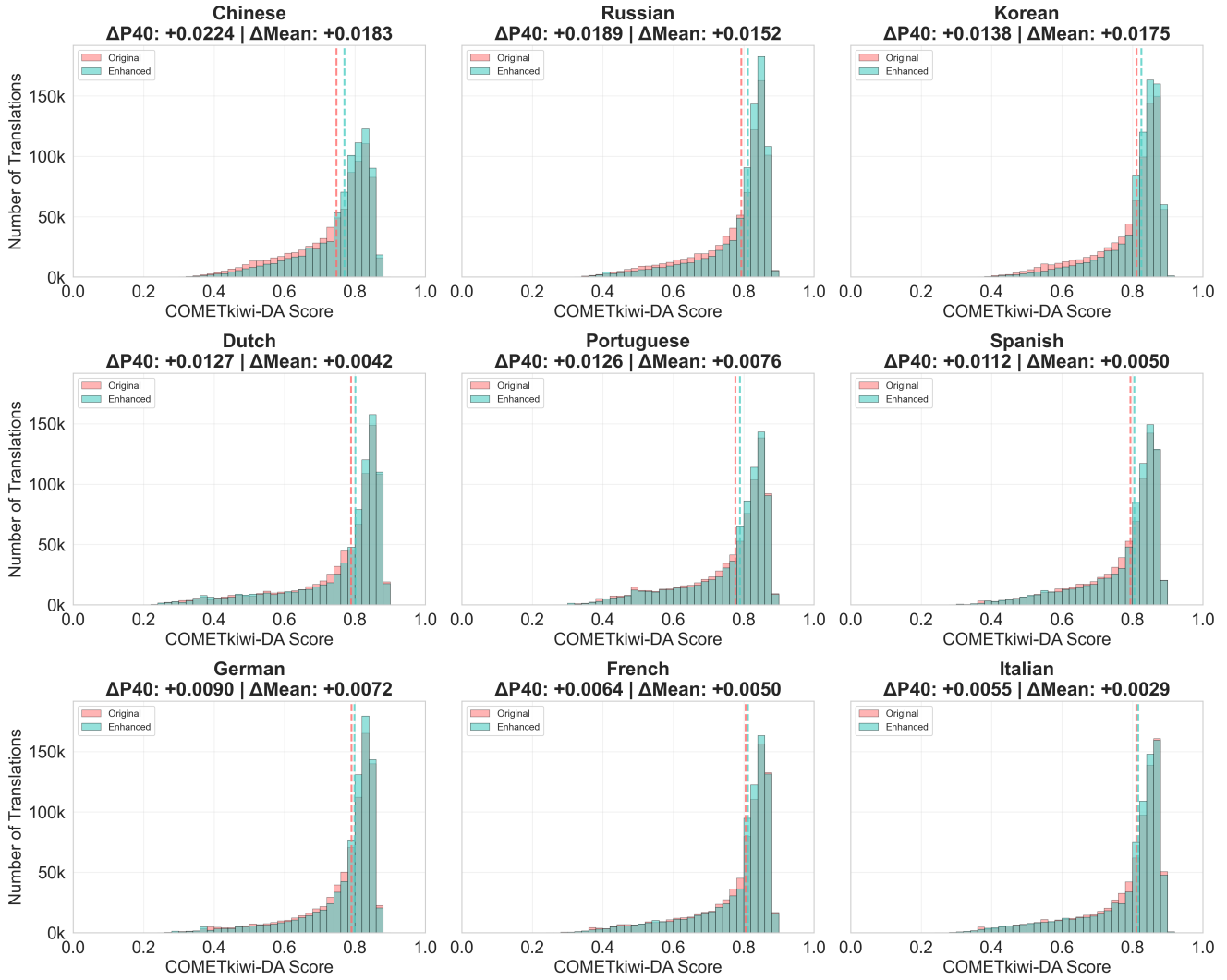


Figure 3. Translation quality distributions before and after visual enhancement for the nine 9 target languages. Each panel shows overlaid histograms of COMETkiwi-DA scores for original (coral) and enhanced (teal) translations. All languages show rightward distribution shifts, with Chinese exhibiting the most substantial improvement.



Figure 4. Multilingual localization consistency demonstrated on a wine tasting scene. The model accurately identifies the second wine glass from the left when queried in Russian (left), English (center), and Italian (right). Despite linguistic variations across three language families (Slavic, Germanic, and Romance), the spatial predictions remain nearly identical, with green boxes indicating the ground truth and red boxes showing the model predictions.



Figure 5. Examples illustrating fine-grained object discrimination in a multi-object scene. Three referring expressions targeting different objects in the same office environment demonstrate compositional reasoning: identifying an earphone by material and color (left), a cup by color and text pattern (center), and a glass container by material properties (right). The model successfully disambiguates targets from distractors using combined attribute descriptions.



Figure 6. Cross-lingual localization consistency for a knife in a plated dish. The model produces spatially consistent predictions across Dutch (left), Portuguese (middle), and Russian (right) referring expressions, all targeting the same knife. Red boxes indicate the predictions, while green boxes show the ground truth. The slight deviation in the Dutch prediction (IoU: 0.784) compared to Portuguese (IoU: 0.771) and Russian (IoU: 0.802) may reflect subtle differences in translation quality or tokenization patterns, but all three achieve strong localization accuracy.

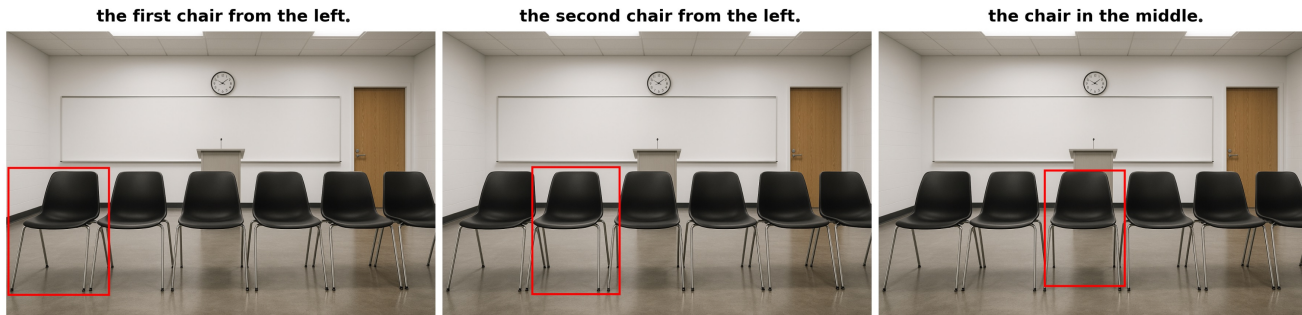


Figure 7. Ordinal reasoning with identical objects. Left: "the first chair from the left", Center: "the second chair from the left", Right: "the chair in the middle". The model successfully performs positional counting to distinguish visually identical chairs based solely on spatial ordering descriptors.



Figure 8. Small object localization examples spanning diverse visual domains. Left: "What works with the engine?" targeting a boat on the Thames River (IoU: 0.669); Center: "The pedestrians walk between parked vehicles" identifying a small human figure in an aerial parking lot view (IoU: 0.553); Right: "What do cats wear for fashion or identification?" localizing a collar on a cat near a laptop (IoU: 0.821). These examples illustrate that localization difficulty correlates with both absolute object size and contextual clutter rather than object category alone.

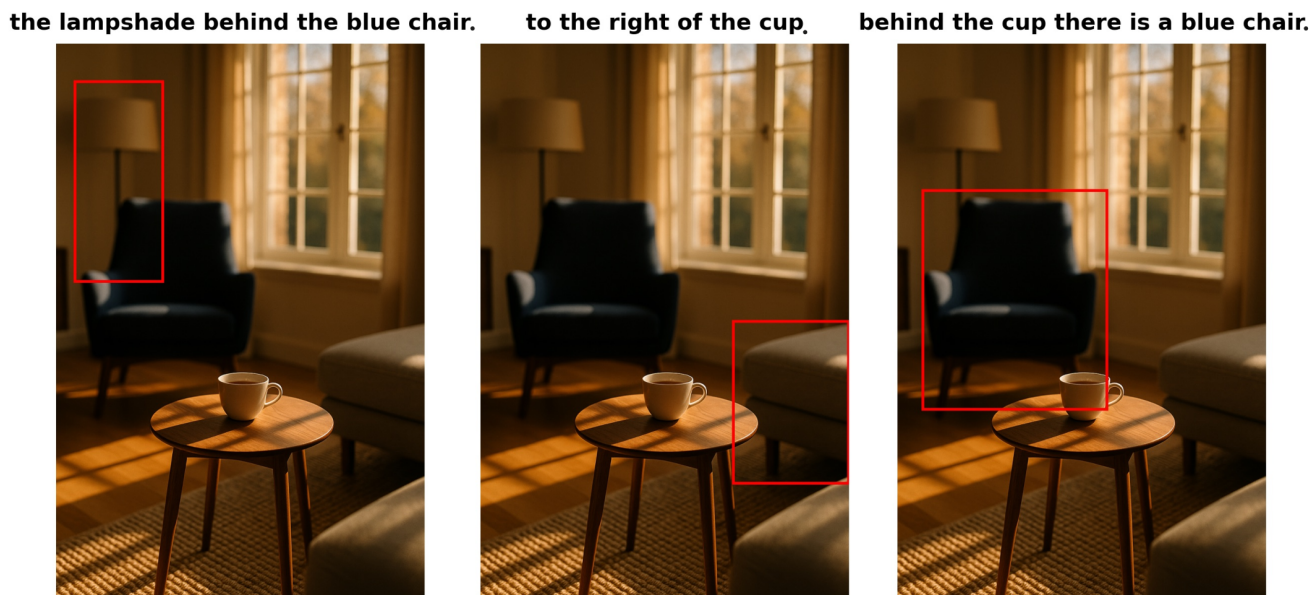


Figure 9. Illustration for multi-hop spatial relationship reasoning. Left: "the lampshade behind the blue chair", Center: "to the right of the cup", Right: "behind the cup there is a blue chair".

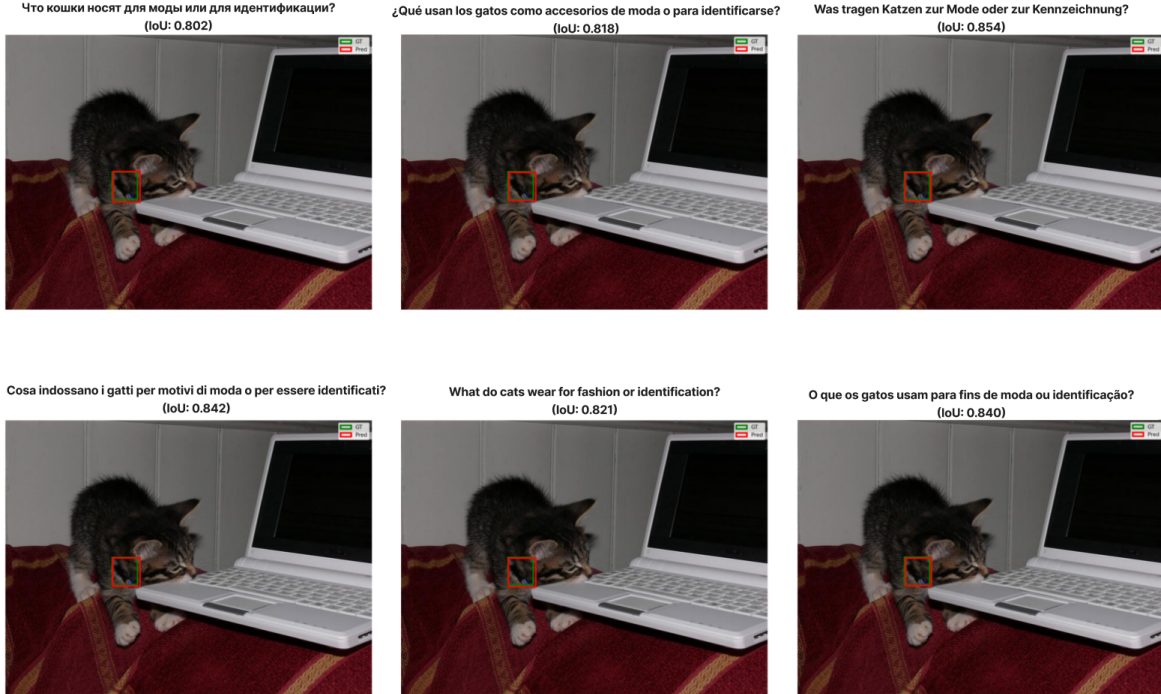


Figure 10. Illustration for small object localization across six languages: Russian, Portuguese, German, Italian, English, and Portuguese. The model successfully identifies a cat’s collar with consistent accuracy across all linguistic variants. The referring expressions all translate to “What do cats wear for fashion or identification?” from the respective languages. The mean IoU across languages: 0.831, demonstrating that small object localization accuracy remains stable in multilingual contexts.

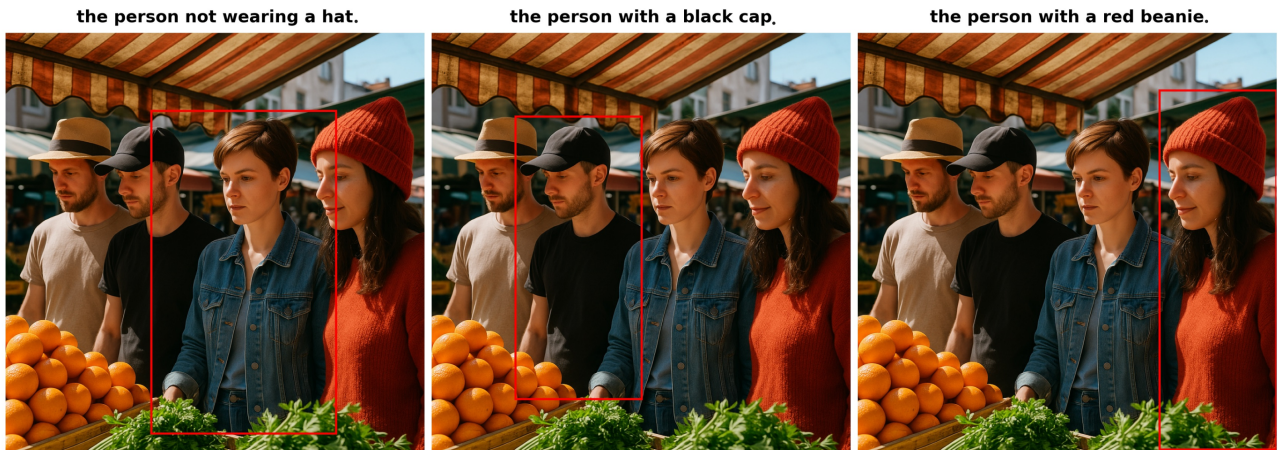
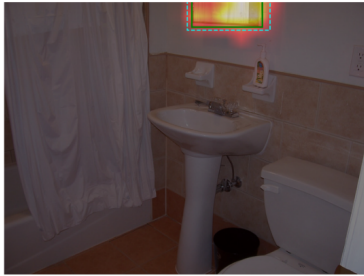


Figure 11. Illustration for negation handling in attribute-based referring expressions. Left: “the person not wearing a hat”, correctly identifies absence of attribute. Center: “the person with a black cap”, positive attribute matching. Right: “the person with a red beanie”, color-specific accessory identification.

A white plastic soap dispenser with a white plastic spout, a green, blue, and light brown paper label. (IoU: 0.683)



A light brown wooden framed mirror. (IoU: 0.736)



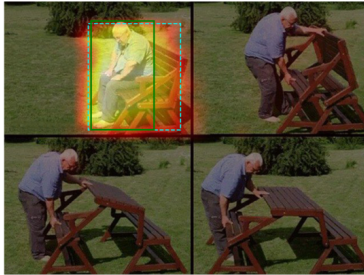
A black trash can. (IoU: 0.751)



the silver car in the background reflecting off of the window. (IoU: 0.895)



Which one contains a man sitting on a bench? (IoU: 0.668)



The red tricycle parks at the bottom-left corner near the building. (IoU: 0.651)

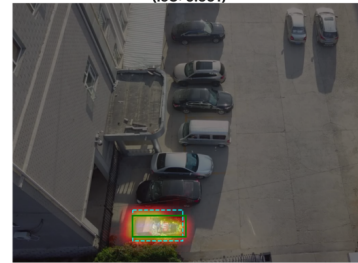
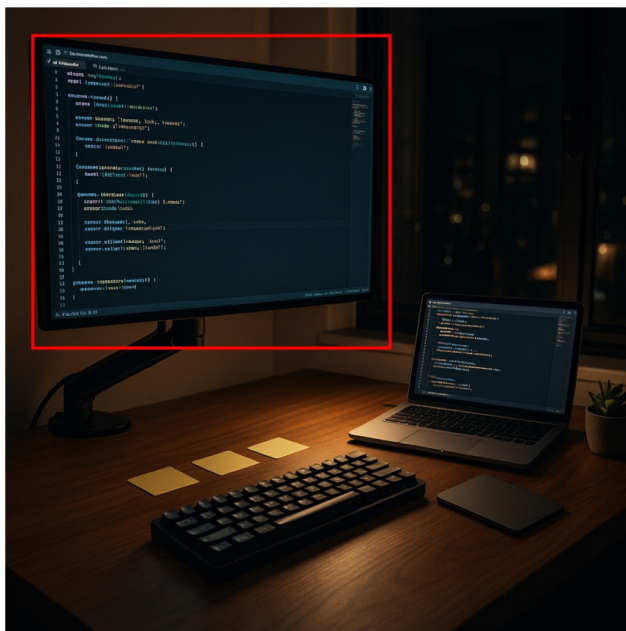


Figure 12. Attention distribution visualizations for five diverse referring expressions. Top row: "A black trash can" (IoU: 0.751), "A light brown wooden framed mirror" (IoU: 0.736), "Which one contains a man sitting on a bench?" (IoU: 0.668). Bottom row: "The red tricycle parks at the bottom-left corner near the building" (IoU: 0.651), "The black cars park along the left side of the parking area" (IoU: 0.755), "A white plastic soap dispenser" (IoU: 0.683).

the large monitor on the left.



the smallest screen.

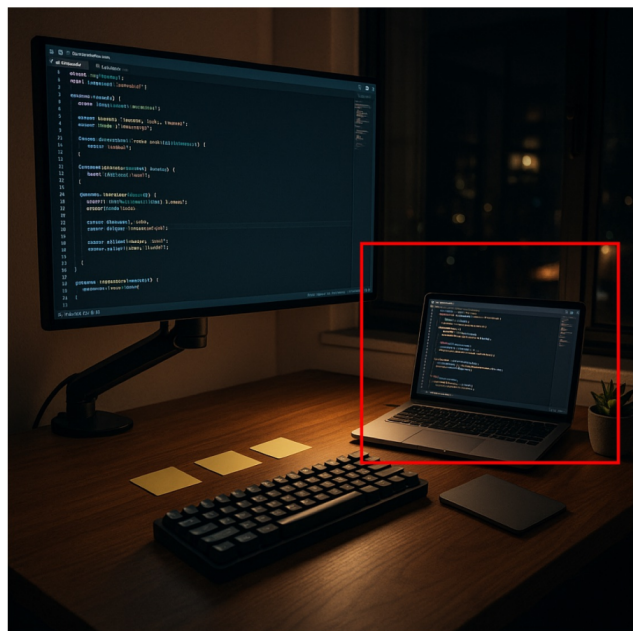


Figure 13. Illustration for relative size discrimination within the same object category. Left: "the large monitor on the left", targets larger desktop display. Right: "the smallest screen", targets laptop display.

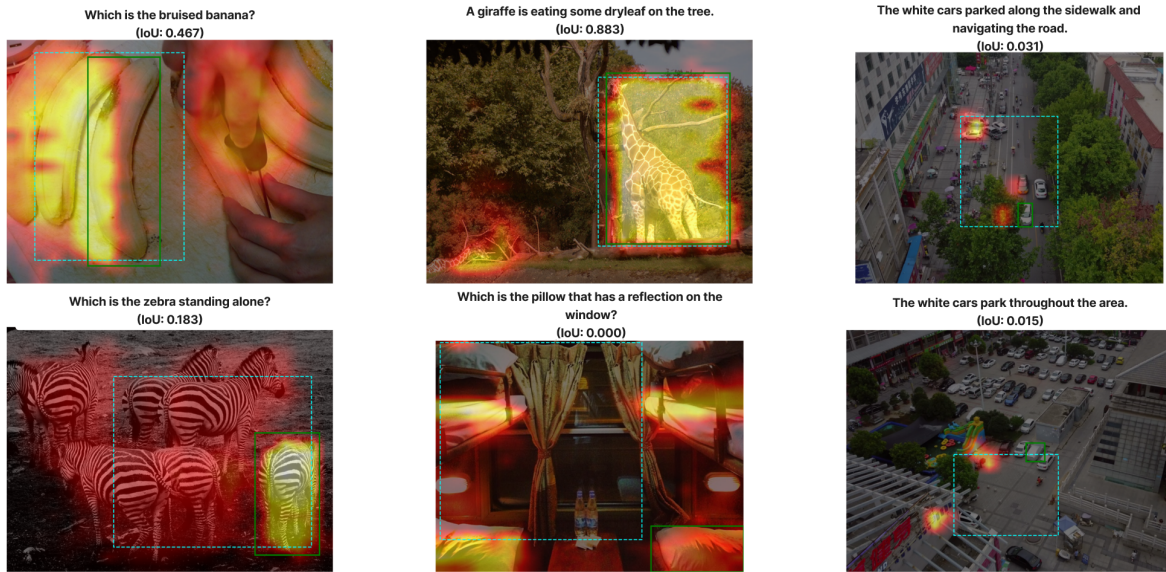
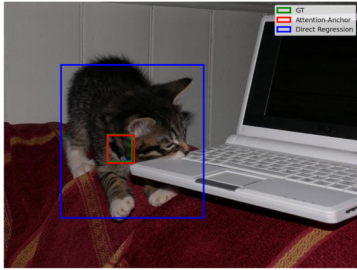


Figure 14. Failure cases illustrating systematic challenges. Top row: "Which is the bruised banana?", "a giraffe is eating some dryleaf on the tree", "The white cars parked along the sidewalk and navigating the road." Bottom row: "Which is the zebra standing alone?", "Which is pillow that has a reflection on the window?", "The white cars park throughout the area."



Figure 15. Illustration for model predictions across challenging scenarios: multiple-choice localization with similar objects (left), fine-grained food item identification (center), and person identification with specific attribute descriptions (right). Green boxes indicate the ground truth, while red boxes show predictions.

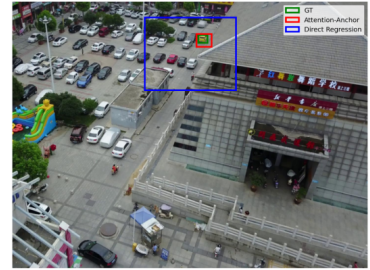
What do cats wear for fashion or identification?
(IoU Attention-Anchor: 0.821 | IoU Direct-Regression: 0.030)



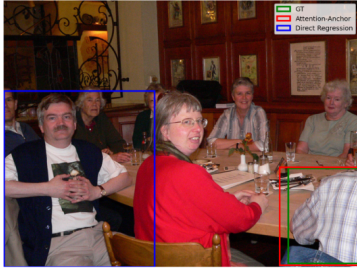
A light brown wooden framed mirror.
(IoU Attention-Anchor: 0.736 | IoU Direct-Regression: 0.318)



The yellow cars park in the lot.
(IoU Attention-Anchor: 0.382 | IoU Direct-Regression: 0.011)



Which person is in the corner wearing a plaid shirt?
(IoU Attention-Anchor: 0.684 | IoU Direct-Regression: 0.000)



Left box labeled 'Golden Curry,' lying on its side.
(IoU Attention-Anchor: 0.860 | IoU Direct-Regression: 0.000)



The box with a bowl and bar code on it.
(IoU Attention-Anchor: 0.840 | IoU Direct-Regression: 0.010)



Figure 16. Qualitative comparison between attention-anchored (red) and direct regression (blue) predictions across six scenarios. Green boxes indicate ground truth. Top row: Small object localization where attention-anchored succeeds while direct regression fails. Bottom row: Cases where attention-anchored maintains strong performance while direct regression exhibits complete failures.

the dark blue car.



the bright blue car.



Figure 17. Illustration for fine-grained color discrimination with scale variation. Left: "the dark blue car" targeting the full-size vehicle with darker blue paint. Right: "the bright blue car" targeting the toy car with lighter blue color.

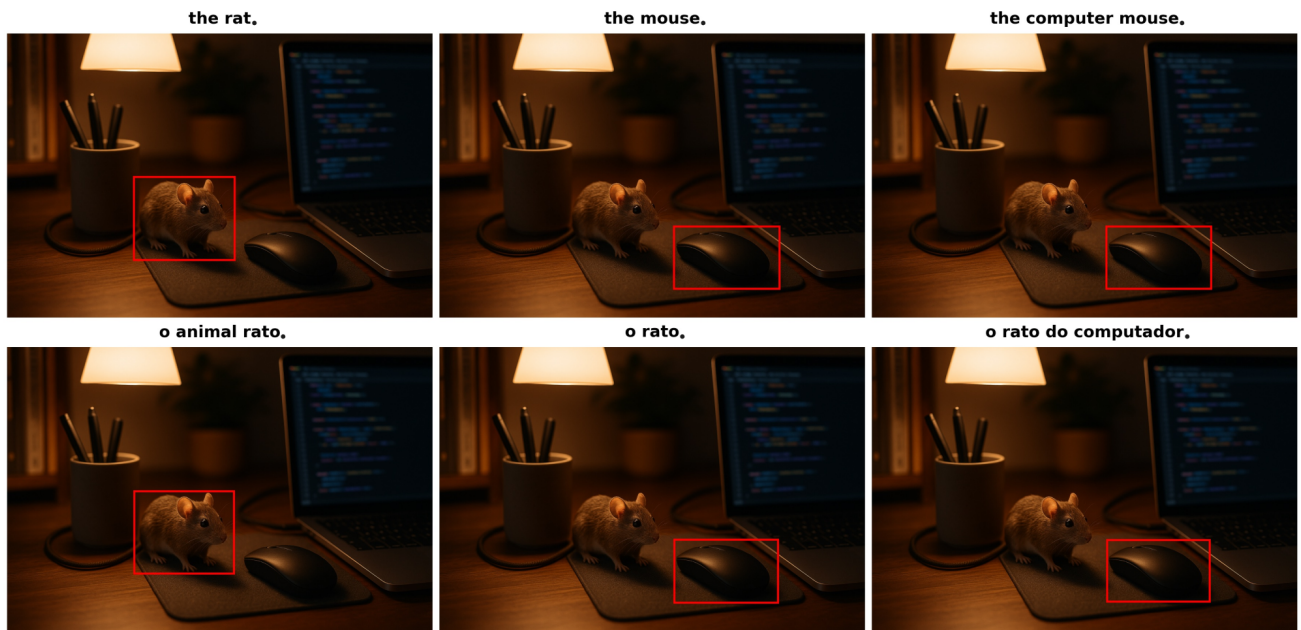


Figure 18. Semantic disambiguation through visual grounding in English and Portuguese. Top row: English “*the rat*” (animal), “*the mouse*” (computer peripheral), and “*the computer mouse*” with explicit category modifier. Bottom row: Portuguese “*o animal rato*” (the animal rat) with category specifier “*animal*”, “*o rato*” requiring visual context for disambiguation, and “*o rato do computador*” (the computer mouse/rat) with explicit qualifier “*do computador*”. The word “*rato*” in Portuguese inherently references both the biological animal and the computer device, necessitating explicit modifiers for unambiguous reference.